PAPER • **OPEN ACCESS**

Numerical investigation of four photovoltaic/thermal integrated structures from energetic point of view

To cite this article: M Abd El-Hamid *et al* 2021 *IOP Conf. Ser.: Mater. Sci. Eng.* **1172** 012018

Numerical investigation of four photovoltaic/thermal integrated structures from energetic point of view

M Abd El-Hamid[1, 2], S Moustafa[1, 2]and G Wei[1]

[1] Key Laboratory of Power Station Energy Transfer Conversion and System of Ministry of Education, School of Energy, Power and Mechanical Engineering, North China Electric Power University, Beijing 102206, China
[2] Mechanical Power Engineering Department, Faculty of Engineering – Mattaria, Helwan University, Cairo 11718, Egypt

E-mail: eng.mohamed.abdelhamed90@gmail.com

Abstract. Photovoltaic/Thermal (PV/T) module is considered to be one of the most recent technologies which offers harness and production of both electric and thermal energy. In the current study an energetic analysis is carried out to compare between four different configurations which are: the single pass single glazed (PV/T-I), the single pass double glazed with air gap (PV/T-II), the single pass double glazed with argon gap (PV/T-III) and the double pass double glazed (PV/T-IV) hybrid photovoltaic/Thermal air collector systems. A 3 dimensional numerical model is built up and validated with both the numerical and experimental results coming from the literature. The numerical simulations have been accomplished to investigate the energetic performance with a detailed thermal and electrical study taking in account an inlet coolant temperature the same as the ambient temperature for a coolant (air) mass flow rate equals to 0.025 kg/s of a typical day in August from 9:00 to 17:00 under the ambient conditions of Beijing, China. The results show that the single pass single glazed configuration has the highest electrical efficiency, whereas the double pass configuration has the greatest thermal and energy efficiencies among the proposed configurations. The average daily energy efficiencies are 53.14%, 75.92%, 77.63% and 82.19% for the (PV/T-I), (PV/T-II), (PV/T-III) and (PV/T-IV) configurations, respectively.

1. Introduction

The lack of energy, along with the environmental challenges associated with conventional energy production using fossil fuels, as well as the rapid growth of the world population, offer a clear motivation for a much extended sustainable energy supply represented in the renewable energy resources [1]. Solar energy is considered to be as the most relevant renewable energy source for the whole world. Solar energy can be captured by two different means separately: the solar photovoltaic system (PV) which transforms the solar energy to an electric power and the solar thermal structure that transforms the solar energy in to a thermal energy. As a result, the photovoltaic thermal hybrid structure (PV/T) is a method in which the PV not only provides electricity but also functions as a thermal absorber by collecting heat from the PV system, resulting in a higher electrical gain.

In the past 50 years, a wide variety of the PV/T investigations have been performed since the early 1970s using water or air as a coolant starting from Wolf [2], Kern and Russell [3] in the early 1970s who use water or air as cooling fluids. Many studies have been implemented in recent decades to boost

the overall energetic efficiency of the PV/T integrated configurations, however, the design and the layers arrangement of a PV/T integrated collector need further improvement to boost the overall efficiency. It was found from the literature review that the coolant passage underneath the proposed PV design achieved the highest overall efficiency among the evaluated different designs of the PV/T structures as shown by Zondag et al. [4]. Using the glazed PV/T configuration for the purpose of water-heating can enhance the thermal efficiency till 30% compared to the unglazed systems as dedicated by Tripanagnostopoulos et al. [5] and observed that, the electrical efficiency was reduced by about 16%.

Joshi et al. [6] gave a thermal performance comparison between two different types of the hybrid PV/T air collector systems, which were the PV module with a glass to tedlar form and the other was glass to glass form under the weather climates of India. In order to improve the thermal and electrical measurement models, a novel PV/T air collector was tested by Sarhaddi et al. [7] with some heat loss coefficient corrections. The study of the uni pass hybrid PV/T and the dual hybrid PV/T configurations with a metal plate and a glass cover at the top was done by Slimani et al. [8]. The findings revealed a significantly higher thermal efficiency, but a significantly lower electrical efficiency of the second configuration. The average energetic efficiency and the annual energy output were found to be the highest for the PV/T dual-pass air collector as concluded by Slimani et al. [9] who investigated a comparative analysis between different four structures: the photovoltaic traditional module, the PV/T conventional structure, the integrated PV/T dual-pass structure and the PV/T double glazing structure.

Latterly, Sainthiya et al. [10] have studied the effect of cooling the upper surface of the hybrid PV/T collector by water numerically and experimentally under the Indian weather conditions. Recently, an electrical and thermal performances of PV/T air configuration which had one-pass and dual-flow air passage have been proposed experimentally by Choi et al. [11], and it was found that the overall energetic efficiency increased with rising the coolant flow rate, a slight enhancement in the electrical efficiency and significant increase in the thermal efficiency were induced.

According to the previous literature review, it will be an effective study to concentrate on the influence of adding an upper glass layer for single pass configurations with a static air or argon above the PV structure and use a double pass channel for the cooling fluid of PV/T configurations, that may enhance the overall energetic performance of the hybrid PV/T configuration. Thus, a thermal and electrical performance investigation performed in the current study to compare between different four configurations, which are: the single pass single glazed (PV/T-I), the single pass double glazed with air gap (PV/T-II), the single pass double glazed with argon gap (PV/T-III) and the double pass double glazed (PV/T-IV) hybrid photovoltaic/Thermal air collector systems.

2. System design and description

In the current study four PV/T structures are numerically analyzed and compared. The proposed hybrid PV/T configurations are using glazed PV module with different positions of cooling channels as illustrated in Fig. 1. The PV module is of mono-crystalline type with 50 watt maximum power rating as released by the manufacturer [12]. The first configuration is the single pass single glazed module (PV/T-I) which is composed of: the PV and an air passage beneath the PV module with an aluminum absorber plate attached under the air duct. The tedlar layer below the PV cells and the top glass cover both act as protective layers. The aluminum absorber plate is to lower the temperature of the module through the convective and radiative heat transfer [9].

The second configuration is the single pass double glazed with air gap module (PV/T-II) which is the same as the first configuration, but with adding confined air gap above the PV module and enclosing this gap with an upper protective glass layer. The third configuration is the single pass double glazed with an argon gap module (PV/T-III) with the same layers as the second configuration but with the confined gap filled with argon instead of air. Whereas, the fourth configuration is the double pass with double glazed module (PV/T-IV) consisting of top glass cover with dual air passages; one above the PV module and the other is underneath it attached to an aluminum absorber plate as seen in Fig. 1.

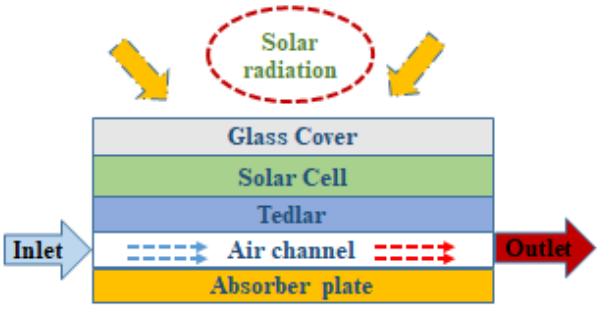

Single pass single glazed structure (PV/T-I)

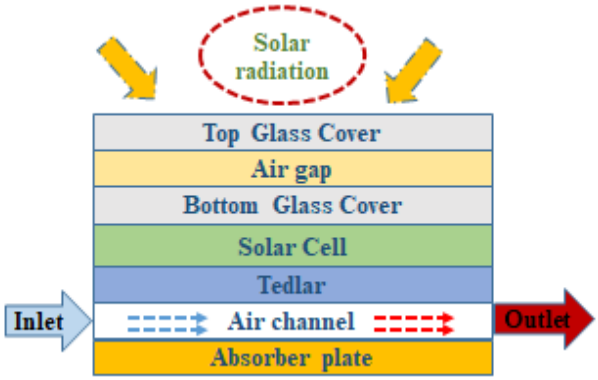

Single pass double glazed structure with air gap (PV/T-II)

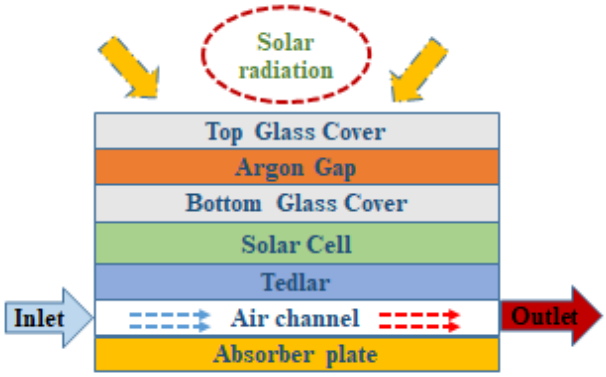

Single pass double glazed structure with argon gap (PV/T-III)

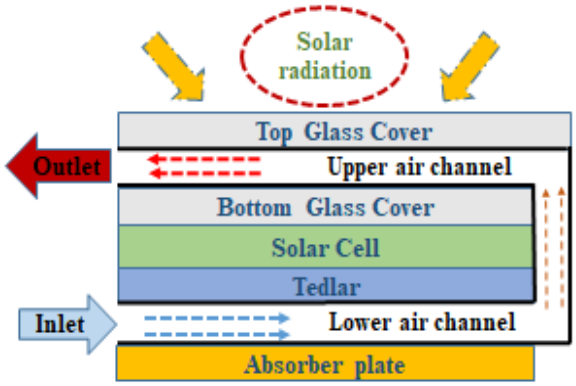

double pass double glazed structure (PV/T-IV)

Figure 1. Schematic diagram of the suggested hybrid PV/T air collector configurations.

3. Numerical analysis

The governing equations, the boundary conditions, the proposed model accuracy including the mesh independence test and the ambient conditions for the current study are presented in this section.

3.1. Governing equations and performance evaluation parameters

In the current study, a three-dimensional numerical model is established and simulated by using ANSYS FLUENT 19.1. The governing equations can be derived as:

Continuity equation:

$$\nabla.(\rho\vec{V}) = 0 \tag{1}$$

Momentum equation:

$$\vec{V}.\nabla(\rho\vec{V}) = \nabla P + \nabla.(\mu\nabla\vec{V}) \tag{2}$$

Energy equation for the cooling fluid:

$$\vec{V}.\nabla\left(\rho C_p T_f\right) = \nabla .(k_f \nabla T_f) + \nabla q_{rad} \quad (3)$$

Energy equation for the PV/T module layers:

$$\nabla .(k_f \nabla T_f) + \nabla q_{rad} = 0 \quad (4)$$

where $\vec{V}$, P, μ, ρ, C_p, k_f and T_{f} are the symbols for the velocity vector, pressure, dynamic viscosity, density, specific heat at constant pressure, thermal conductivity and temperature of the cooling fluid, respectively. q_{rad} refers to the radiative energy net loss through a control volume and named as the radiative term which equals to the absorbed incident radiation on a control volume subtracted from the emitted energy from that volume.

In order to investigate the system performance, the thermal efficiency, electrical efficiency and overall energetic efficiency is evaluated according to Eqs. (5), (8) and (10), respectively.

$$\eta_{th} = \frac{E_{th}}{E_s} \quad (5)$$

where E_{s} is the total energy coming from solar radiation. E_{th} is the absorbed thermal energy by the coolant, which is air in the current work. E_{s} and E_{th} are calculated as Eqs. (6) and (7), respectively.

$$E_s = G\ A_s \quad (6)$$

where G is the radiation intensity per unit area and A_{s} is the net absorbed surface area of PV module.

$$E_{th} = \dot{m}\ C_p\ (T_{out} - T_{in}) \quad (7)$$

where $\dot{m}$, C_{p}, $T_{o\mathrm{ut}}$ and $T_{i\mathrm{n}}$ are the mass flow rate, specific heat capacity, outlet temperature and inlet temperature of the coolant (air) , respectively.

$$\eta_{ele} = \frac{E_{ele}}{E_s} = \eta_{ref}([1 - \delta_{sc}(T_{sc} - T_{ref})] \quad (8)$$

$$E_{ele} = \eta_{sc}\ A_{sc}\ \ G_{sc}\ [1 - \delta_{sc}(T_{sc} - T_{ref})] \quad (9)$$

where E_{ele} is the produced electric power from the PV module, η_{sc} refers to the PV cell efficiency at standard temperature, A_{sc} is the PV cell surface area, G_{sc} is the portion of incoming solar radiation that reaches to the PV cell by taking in account both the solar cell absorptivity, the above layers transmissivity and the PV module packing factor, δ_{sc} refers to the temperature coefficient of the mono crystalline silicon cell which can be taken as 0.45%, T_{sc} and T_{ref} are the solar cell temperature and the reference temperature, respectively.

The overall energetic efficiency (η_o) for the hybrid system can be deduced by adding both electrical and thermal efficiencies as follows:

$$\eta_o = \eta_{\mathrm{ele}} + \eta_{\mathrm{th}} \quad (10)$$

3.2. Boundary conditions

A thermal coupled boundary condition for solid-solid interface in PV/T systems is employed as:

$$(k_o \nabla T_o) = (k_{ó} \nabla T_{ó}) \quad (11)$$

where *k* refers to the thermal conductivity, subscripts o and $ó$ refer to the proposed layer and the upper layer or the layer beneath it. For the solid-fluid interface, the no slip condition is applied as:

$$u=v=w=0, \qquad T_{air} = T_{duct} \quad (12)$$

The boundary conditions at both the inlet and outlet sections of the air channels are as follows:

$$w=w_{in}, \qquad T=T_{in}, \quad (13)$$

$$P_o = 0\ (gage) \quad (14)$$

Eq. (15) represents the calculation method of the hydraulic diameter and the turbulence intensity at both inlet and outlet sections of the air duct, which are activated on using the K-epsilon turbulence model used in the current study [13] :

$$D_h = \frac{2\,(L_{duct} \times B_{duct})}{(L_{duct} + B_{duct})}, \qquad z = 0.16\, Re^{-1/8} \quad (15)$$

where D_{h} refers to the hydraulic diameter, L_{duct} refers to the duct length, B_{duct} is the duct width, z refers to the turbulence intensity and Re is Reynolds number. By treating each layer in PV/T hybrid system as a control volume, the energy is gained by conduction from the above layer and by radiation via the reached portion of solar radiation to this layer, which is calculated according to the absorptivity of this layer and the transmittance of the above layer to the incoming solar radiation according to thermal and optical properties stated in Table 1 and 2.

Table 1. Dimensions and thermal properties of the used materials.

Layer	Dimensions (mm)	Density (kg/m^3)	Thermal conductivity (W/m K)	Specific heat (J/kg K)
Top and bottom Glass covers	1280×320×3.2	2770	2	500
Solar cell	1280×320×0.3	2330	148	677
Tedlar	1280×320×0.5	1200	0.15	1250
Air duct (Aluminum)	1280×300×20	2719	202.4	871
Aluminum plate	1280×300×2	2719	202.4	871

Table 2. Optical properties of the used materials [14].

Layer	Reflectivity	Absorptivity	Transmissivity	Emissivity
Glass	0.04	0.04	0.92	0.85
Solar cell	0.08	0.90	0.02	-
Aluminum	-	-	-	0.90

3.3. Mesh independence study

In order to check the grid independence test, ten mesh systems are done with different cell numbers for a PV/T module with the same dimensions and material properties as the PV/T module that was investigated by Joshi et al. [6]. The grid independence test is conducted by applying 600 W/m2 radiation heat flux, 300 K ambient temperature, 300 K cooling fluid inlet temperature and 1/m/s wind velocity. It

can be seen that the solution represented in both solar cell and cooling fluid outlet temperatures becomes independent on grid size after 2,116,851 elements as illustrated in Fig. 2.

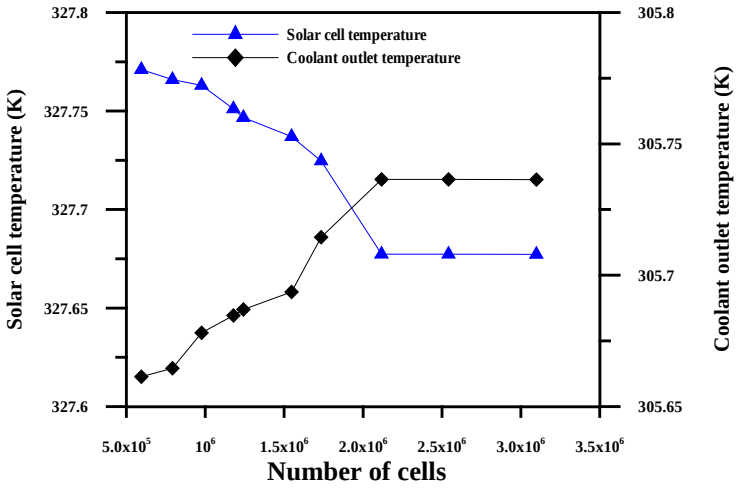

Figure 2. Mesh independence test for solar cell and coolant outlet temperatures.

3.4. Model validation

The present numerical work has been validated with both numerical and experimental works that has been carried out by Joshi et al. [6] and numerical results investigated by Slimani et al. [9] and Sarhaddi et al. [7] at an identical ambient and operating conditions. The validation is carried out to verify the accuracy of the current numerical model. The numerical data for the solar cell temperature of the present numerical model achieves a maximum errors of 6%, 7.5%, 16.5% and 17.5% ,but the maximum errors attained through the present work for the coolant outlet temperature are 5.8%, 1.8% , 7.4% and 1.7% with Joshi et al. [6] experimental study, Slimani et al.[9], Sarhaddi et al. [7] and Joshi et al. [6] predicted results, respectively, as displayed in Fig. 3 (a) and (b).

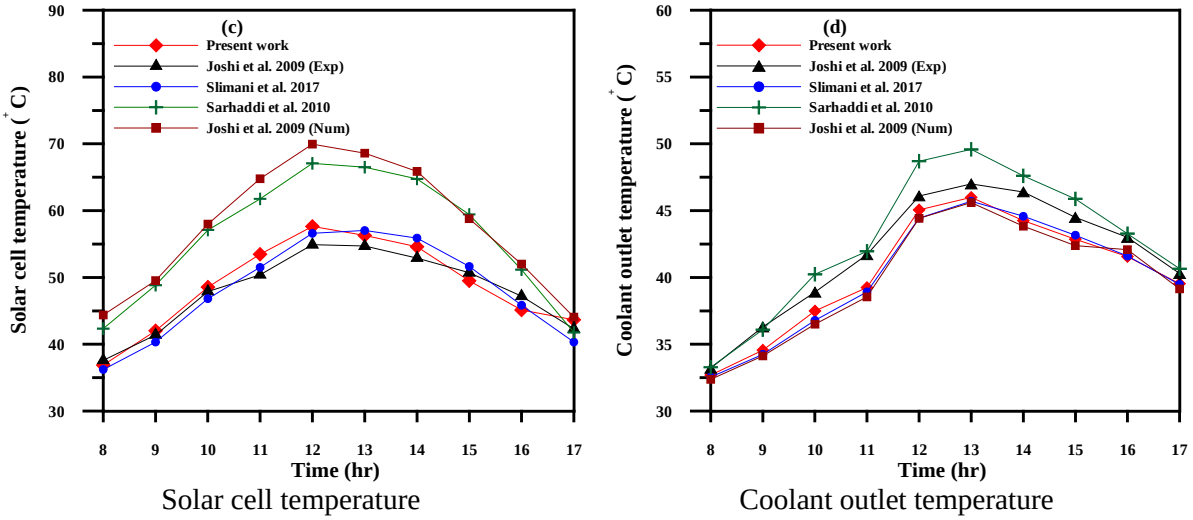

Figure 3. Comparison of the present numerical work with the previous work hourly.

3.5. Weather conditions

Figure 4 gives the typical weather conditions in August of Beijing, China. These data is used in the following numerical simulations.

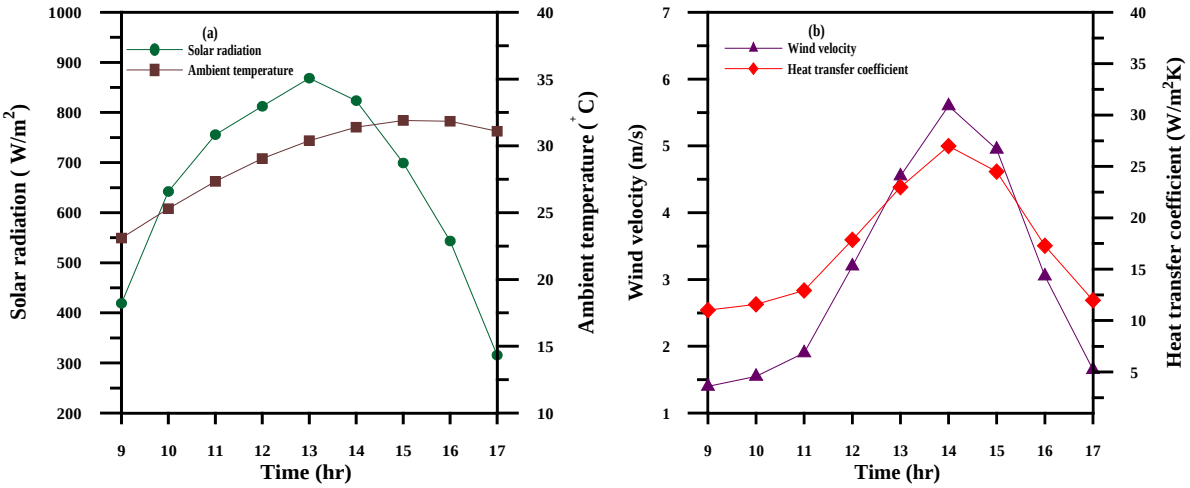

Solar radiation and ambient temperature Wind velocity and heat transfer coefficient

Figure 4. Variations of the solar radiation and the ambient temperature for a typical day in August.

4. Results and discussion

In this section the temperature gradient of the layers and the energetic performance of the four proposed configurations are numerically investigated with an air mass flow rate of 0.025 kg/s and the temperature of the incoming coolant is the same as the ambient temperature for a certain day in Beijing, China, in August.

4.1. Temperature distribution

Figure 5 represents the temperature change with time of the suggested four configurations. It is depicted that the highest temperatures occur under the highest solar radiation intensity, which has a major effect rather than wind speed and ambient temperature for all layers, except for the temperature of air outlet and the top glass layer. The temperatures of air outlet and the top glass layer are apparently affected by the wind velocity rather than the incoming solar radiation. The PV cell layer has the highest temperature among all layers for all configurations and the daily peak values are 345.46, 344.55, 324.14 and 323.32 K for the (PV/T-III), (PV/T-II), (PV/T-I) and (PV/T-IV) configurations, respectively. However, the highest daily outlet air temperatures are 312.97, 313, 312.8 and 308.42 K for the (PV/T-IV), (PV/T-III), (PV/T-II) and (PV/T-I) configurations, respectively.

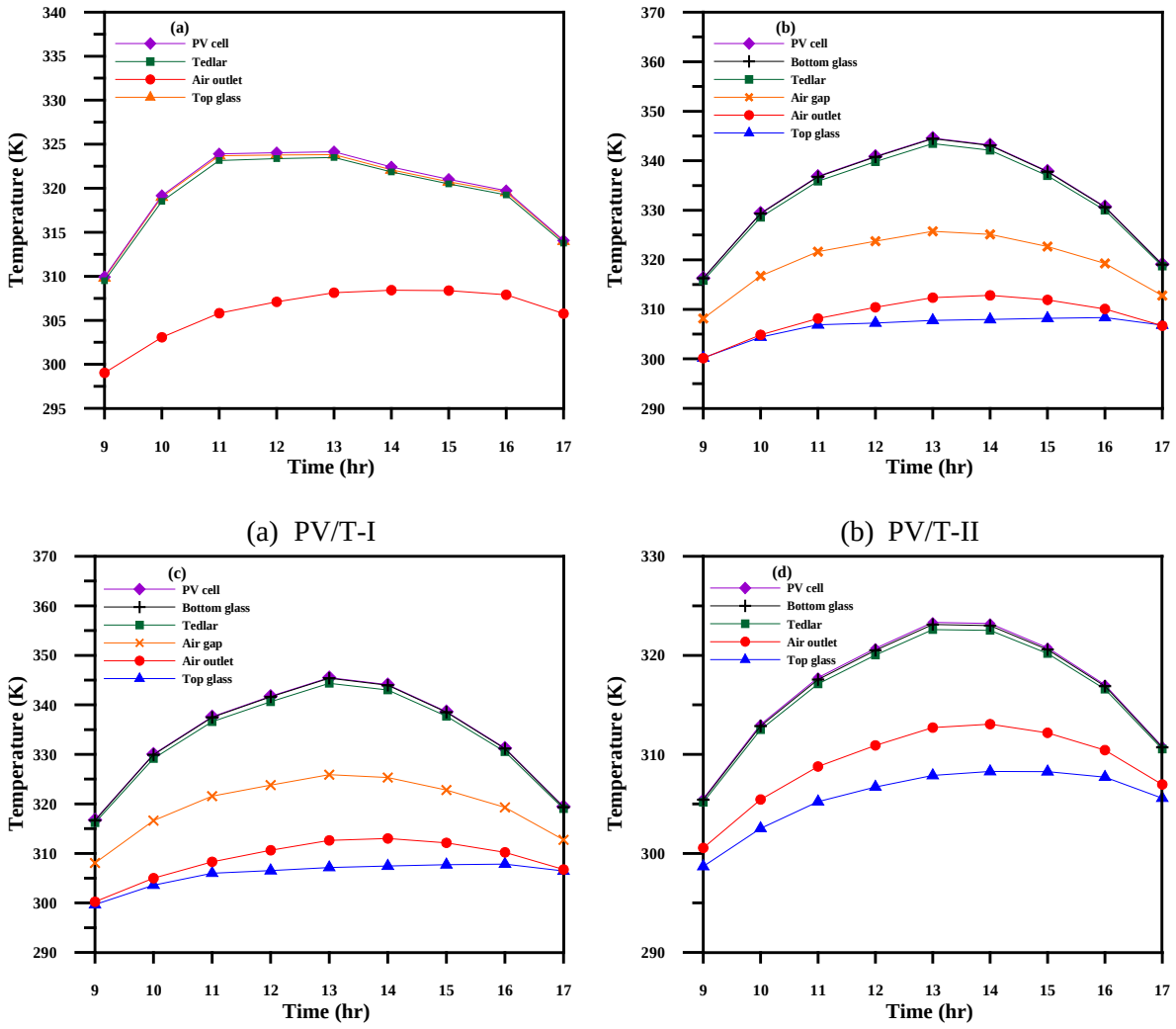

(a) PV/T-I (b) PV/T-II

(c) PV/T-III (d) PV/T-IV

Figure 5. Temperature variation manners at different positions with time of the four PV/T configurations.

Figure 6 displays the temperature distribution contours along the surface of the PV cell layer. It is plain from these contours that, for all designs, the natural convection at the edges of the PV surface is not effective near the inlet portion of the air channel. However, the natural convection effect at the edges of the PV surface begins to increase gradually when the cooling fluid begins to remove the heat from the PV cell layer as it goes far from the inlet section of the air passage. At mid parts, the temperature of the PV surface is significantly higher than that at the edges of the PV surface, as the natural convection effect at the edges of PV surface is stronger than the forced convection effect of the cooling fluid which is air in the present study. The temperature of the PV surface ranges from 318 to 326 K, 326 to 352 K, 326 to 354 K and 316 to 325 K for the (PV/T-I), (PV/T-II), (PV/T-III) and (PV/T-IV) configurations, respectively.

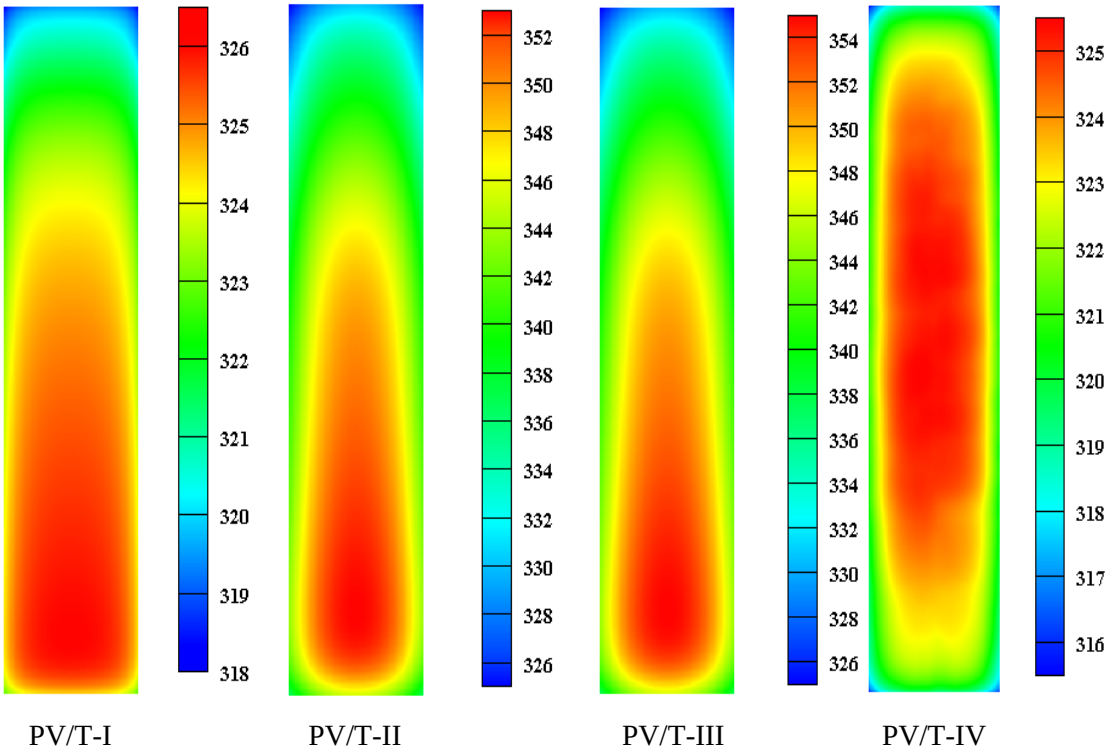

Figure 6. Contours of PV cell surface temperature for all configurations.

4.2. Energetic performance

Figure 7 displays the hourly changes of the thermal power and the electrical power for all the suggested PV/T structures. It is apparent from Fig. 7 (a) that the thermal power marginally increases with increasing the incident solar radiation, as the coolant at the air duct outlet section induces higher temperatures. The highest thermal power values for all configurations are at 13:00 o'clock corresponding to the highest solar radiation, except for the (PV/T-I) configuration the highest thermal power happens at 11:00 o'clock, due to minimizing the layers of this configuration causes the major effect of the wind velocity rather than the solar radiation intensity. The highest thermal power is 240.47 W for the (PV/T-IV) configuration, followed by 238.43, 231.19 and 140.98 W for the (PV/T-III), (PV/T-II) and (PV/T-I) configurations, respectively.

It is shown from Fig. 7 (b) that the highest daily electrical power is reached at 13:00 o'clock corresponding to the maximum daily solar radiation for all the suggested structures. The highest electrical power is 41.65 W for the (PV/T-I) configuration, followed by 35.73, 30.03 and 29.8 W for the (PV/T-IV), (PV/T-II) and (PV/T-III) configurations, respectively.

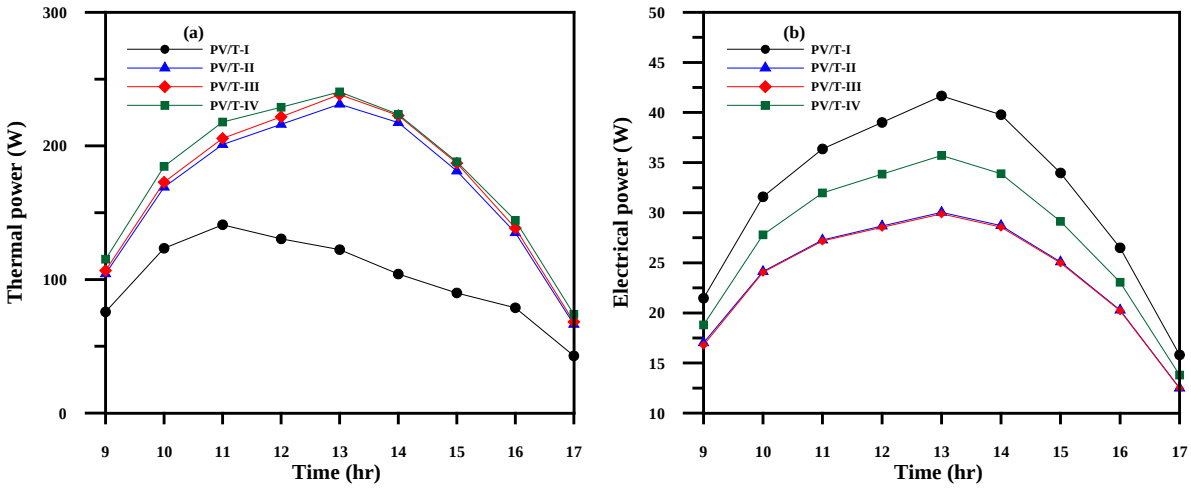

(a) Thermal power (b) Electrical power

Figure 7. Variations of (a) thermal power and (b) electrical power with time.

Figure 8 presents the electrical, thermal and overall energetic efficiencies change with time for all configurations. It is shown in Fig. 8 (a) that the electrical efficiency dramatically decreases with increasing the solar radiation intensity that consequently increase the PV cell temperature. Else, the electrical efficiency reaches its minimum value at 13:00 o'clock corresponding to the highest PV cell temperature for all configurations. It is illustrated in Fig. 8 (a) that the (PV/T-I) configuration offers the highest daily electrical efficiency with a values ranging from 12.49 to 13.33% followed by the (PV/T-IV), (PV/T-II) and (PV/T-III) configurations, with values variation from 10.89 to 12.05%, 9 to 10.57% and 8.95 to 10.42%, respectively.

It can be deduced from Fig. 8 (b) that for the (PV/T-I) and (PV/T-IV) structures the highest daily thermal efficiency is not corresponding to the peak solar radiation time confirming that the wind velocity effect appears significantly more than the solar radiation intensity with different percentages, however for the (PV/T-II) and (PV/T-III) structures the highest daily thermal efficiency is corresponding to the highest daily solar radiation, meaning that, the solar radiation has a greater effect more than the influence of the wind velocity on both modules. The highest daily thermal efficiency is 75.05% for the (PV/T-IV) configuration, followed by 71.48, 69.31 and 50% for the (PV/T-III), (PV/T-II), (PV/T-I) configurations, respectively.

It is obvious from Fig. 8 that the thermal efficiency has the major effect on the behavior of the overall energetic efficiency with a slight contribution by the electrical efficiency for all the designed structures. The overall energetic efficiency values range from 72.86 to 86.4%, 66.7 to 80.44%, 65.1 to 78.68% and 45.47 to 62.83% for the (PV/T-IV), (PV/T-III), (PV/T-II) and (PV/T-I) structures, respectively, as presented in Fig. 8 (c).

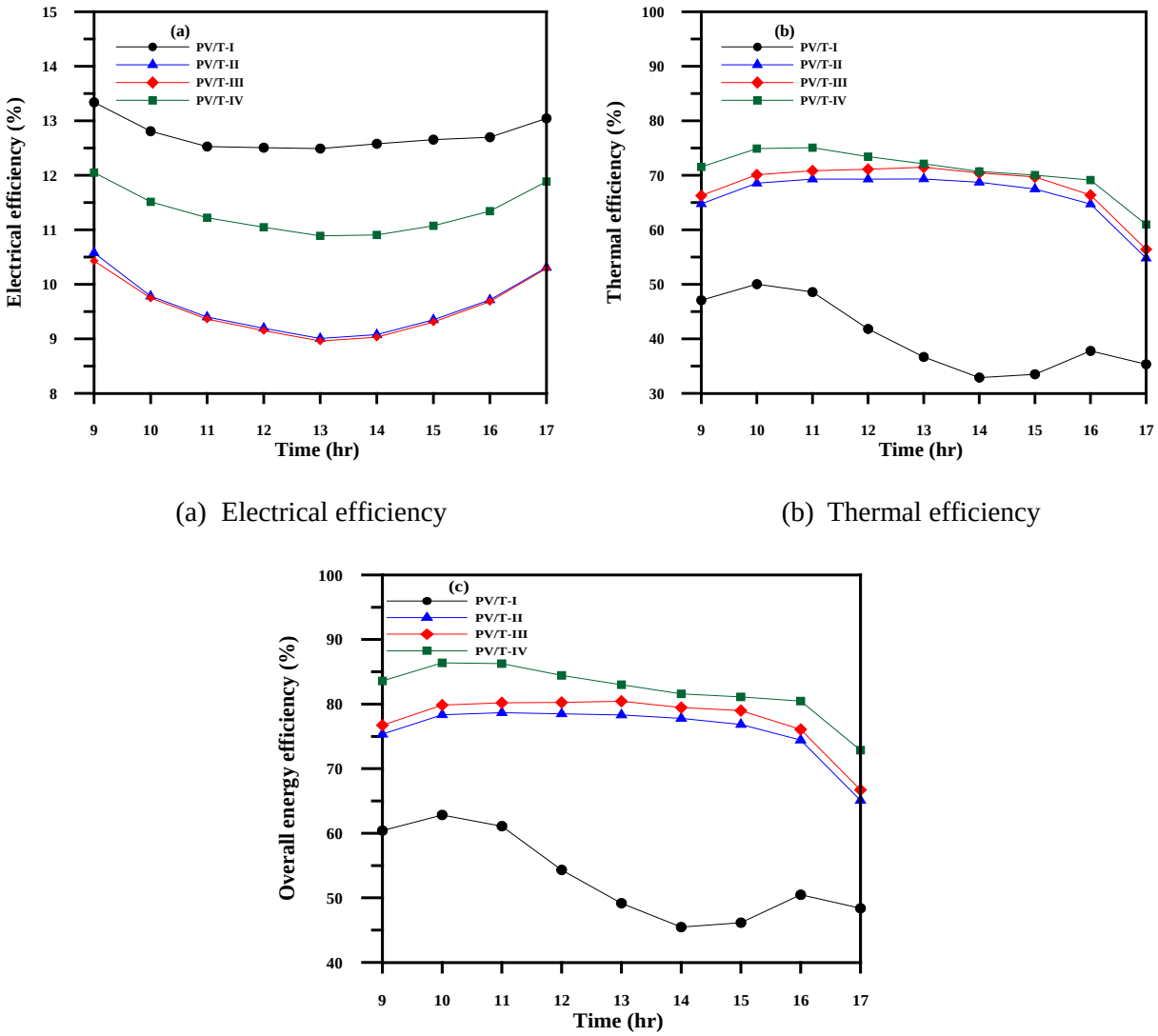

(a) Electrical efficiency

(b) Thermal efficiency

(c) Overall energetic efficiency

Figure 8. Variations of (a) electric efficiency, (b) thermal efficiency and (c) overall energetic efficiency with time for all suggested configurations.

Figure 9 investigates the daily average electrical, thermal and overall energetic efficiencies for each configuration. It is evident from this figure that the contribution of the thermal efficiency is somewhat superior to the electrical efficiency, due to the performance evaluation using the energetic concept accounts for the quantity of energy only as stated by the thermodynamics first law. The percent of share for the average daily thermal efficiency in the average daily overall energy efficiency is 86.2, 87.69, 87.35 and 76% for the (PV/T-IV), (PV/T-III), (PV/T-II) and (PV/T-I) configurations, respectively.

Figure 10 demonstrates the thermal and electrical energy outputs for each configuration. It is clearly shown that the highest average daily energy output is for the (PV/T-IV) configuration with a value of 4856.7 Wh/m^2 followed by the (PV/T-III), (PV/T-II) and (PV/T-I) structures with values of 4614.27, 4519.6 and 3111.32 Wh/m^2, respectively.

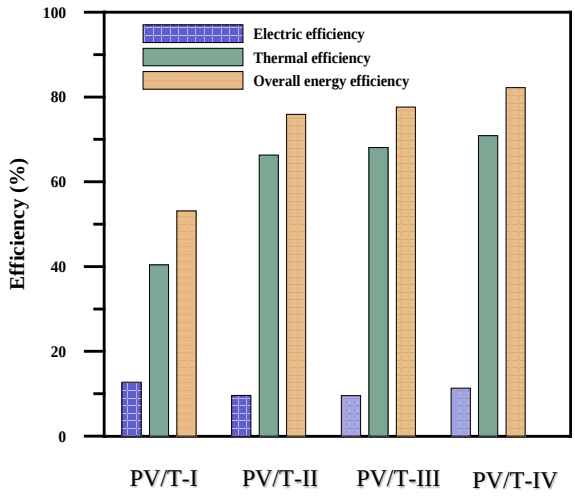

Figure 9. Daily average electrical, thermal and overall energy efficiencies for each configuration.

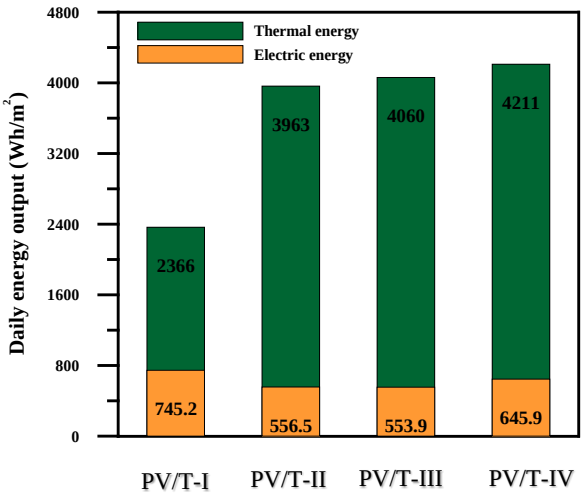

Figure 10. Daily thermal and electrical energy output for each configuration.

5. Conclusions

To assess the PV/T system energetic performance, four PV/T configurations have been investigated and studied numerically in the current work by considering a typical day of ambient conditions of Beijing, China in August. The following points can be concluded:

- The thermal and energetic efficiencies for the double pass configuration are the highest among the suggested structures.
- The single pass single glazed structure offers the highest electrical efficiency, in contrast the lowest thermal efficiency is achieved among the proposed structures.
- The overall energetic efficiency increases by adding a glass cover at the top surface of the PV module and marginally increases with a double passage of the coolant.
- Using argon instead of air as a gap between the PV module dramatically increases the thermal efficiency and the output, but both the electrical efficiency and the output are silghtly decreased, consequently raising the daily overall energy efficiency and the output.
- The double pass configuration exhibits the highest daily overall energetic efficiency by 82.19% followed by the double glazed with an argon gap, double glazed with air gap and single glazed structures with values of 77.63, 75.92 and 53.14%, respectively.

Acknowledgement

This research was financially supported by the National Natural Science Foundation of China (No. 51776066 and No.51806064).

References

[1] Grossman G and Zaltash A 2001 Absim—modular simulation of advanced absorption systems Int. J. Refrig. **24** 531-543.
[2] Wolf M 1976 Performance analyses of combined heating and photovoltaic power systems for residences *Energy Convers.* **16** 79-90.
[3] Kern J and Russell M 1978 Combined photovoltaic and thermal hybrid collector systems *13th IEEE Photovoltaic Spec. Conf.* 1153-1157.
[4] Zondag H, De Vries D, Van Helden W, Van Zolingen R, and Van Steenhoven A 2003 The yield of different combined pv-thermal collector designs *J. Sol. Energy* **74** 253-269.
[5] Tripanagnostopoulos Y, Nousia T, Souliotis M and Yianoulis P 2002 Hybrid photovoltaic/thermal

solar systems *J. Sol. Energy* **72** 217-234.
[6] Joshi A, Tiwari A, Tiwari G, Dincer I and Reddy B 2009 Performance evaluation of a hybrid photovoltaic thermal (pv/t)(glass-to-glass) system *Int. J. Therm. Sci.* **48** 154-164.
[7] Sarhaddi F, Farahat S, Ajam H, Behzadmehr A and Adeli M 2010 An improved thermal and electrical model for a solar photovoltaic thermal (pv/t) air collector *Appl. Energy* **87** 2328-2339.
[8] Slimani M, Amirat M and Bahria S 2015 Analysis of thermal and electrical performance of a solar pv/t air collector: energetic study for two configurations *3rd Int. Conf. Control Eng. & Info. Technol.* 1-6.
[9] Slimani M, Amirat M, Kurucz I, Bahria S, Hamidat A and Chaouch W 2017 A detailed thermal-electrical model of three photovoltaic/thermal (pv/t) hybrid air collectors and photovoltaic (pv) module: comparative study under algiers climatic conditions *Energy Convers. Manag.* **133** 458-476.
[10] Sainthiya H and Beniwal N 2019 Efficiency enhancement of photovoltaic/thermal (pv/t) module using front surface cooling technique in winter and summer seasons: an experimental investigation *J. Energy Resour. Technol. Trans. ASME* **141** 091201.
[11] Choi H and Choi K 2020 Performance evaluation of pv/t air collector having a single-pass double-flow air channel and non-uniform cross-section transverse rib *Energies* **13** 2203.
[12] Siemens solar industries 2009 Siemens solar module SP50 <www.siemenssolar.com>.
[13] Mohammadi B and Pironneau O 1993 Analysis of the k-epsilon turbulence model.
[14] Zhou J, Yi Q, Wang Y and Ye Z 2015 Temperature distribution of photovoltaic module based on finite element simulation *J. Sol. Energy* **111** 97-103.